Detection of Underground Anomalies Using Analysis of Ground Penetrating Radar Attribute

Cuong Van Anh LE[*1,2)], *Thuan Van NGUYEN*[1,2)]

[1)] University of Science, Ho Chi Minh City, Vietnam
[2)] Vietnam National University Ho Chi Minh city, Ho Chi Minh City, Vietnam
* Corresponding author: lvacuong@hcmus.edu.vn

http://doi.org/10.29227/IM-2020-01-04

Submission date: 02-12-2019 | Review date: 22-01-2020

Abstract

Need of specifying underground construction works for supporting further tasks as maintenance, repairing, or setting up new underground structures. For these needs, ground penetrating radar, one of the efficient geophysical methods, can bring high-resolution and quick underground image revealing existence of both natural and artificial anomalies. Its fixed receiver-transmitter antennas setting as constant offset is commonly used in urban areas. Conventionally, hyperbolae events are crucial indicator for scattering objects as kinds of pipes, water drainage system, and concrete building structures as well as sink holes. Calculation of their depths and sizes requires migration analysis with the environment velocity. Migrated sections with different velocity show different chaos degrees of transformation from a hyperbola diffraction curve to its focused area. We have researched diagrams of different Ground Penetrating Radar attributes as energy, entropy, and varimax dependent on two variables, velocity and window zone covering diffraction events from a set of synthetic data and real data, in specifying the environment velocity. We have developed a novel technique for evaluation of the ground velocity and object's size by combination of the new varimax diagram and the Kirchhoff migration method. The technique can define contribution of diffracted ground penetrating radar waves for building the diagram after removing the reflection contribution. The synthetic datasets consist of different random background noise levels and expressions of different-sized circular and rectangular pipes. The real data is measured for detecting two underground gas pipes in Ba Ria – Vung Tau province, Vietnam.

Keywords: *migration, velocity estimation, Ground Penetrating Radar attribute*

1. Introduction

Electromagnetic waves propagate through the medium and bounce back to receiver antenna after hitting the boundary of two zones of different electric permittivity. The electromagnetic waves characteristics lead to ability of investigation depth depending on their frequencies and electrically conductivity distribution in shallow surface environment (Doolittle and Collins, 1995, Smith and Jol, 1995). Specifically, "skin effect" shows that the higher frequency Ground Penetrating Radar (GPR) section can illustrate higher resolution images rather than lower frequency GPR ones. However, the lower frequency GPR ones can provide images of deep structures better than the higher frequency ones.

Like seismic, the conventionally processed GPR data and their attributes could illuminate underground hidden geophysical or artificial structures and provide tool for estimation of the environment velocity (Chopra and Marfurt, 2007, Le et al., 2019, Nguyen et al., 2017, Fomel et al., 2007, Khoshnavaz et al., 2016, Tomecka-Suchoń and Marcak, 2015, Ercoli et al., 2014).

The wave propagation velocity can help to correctly map the underground anomalies or structures through a specific processing step, migration. Known electric permittivity parameters are valuable for calculating electromagnetic velocity but it is unavailable where no drill hole is provided. To compensate the limitation, different techniques by analyzing GPR travel-time and amplitude sections are developed. Common Mid-Point (CMP) gather or a prior known object's depth can provide tools to evaluate velocity (Yilmaz, 2001, Sham and Lai, 2016, Forte et al., 2014, Zhao et al., 2015). The constant offset (CO) data section can only utilize diffraction phenomena from small objects or edges of large ones (Yilmaz, 2001, Sham and Lai, 2016, Forte et al., 2014, Zhao et al., 2015). Migration technique can collapse the diffraction hyperbolae into highly energy focus points in which the chosen migrated velocity responds to the environment velocity. In the Kirchhoff migration, summation of seismic amplitudes along a diffraction hyperbola is the secondary source amplitude positioning at the peak of the diffraction hyperbola. The GPR data can take an advantage of the migration technique when sharing the same dynamic characteristics with seismic wave. The hyperbola curves are also function of two-way travel time, velocity, size of diffractor and its depth, and antennas distance in which the velocity is analyzed (Sham and Lai, 2016).

Relationship between migrated velocity and a function of migrated data points over a specified window can form a useful GPR attribute diagram for estimation of environment velocity. The diagram can show its extreme value corresponding to the environment velocity. Entropy and its inverse, varimax, are of great indicator for velocity analysis in both geophysical data, seismic and GPR data (De Vries and Berkhout, 1984, Wiggins, 1978, Prego et al., 2017, Fomel et al., 2007, Levy and Oldenburg, 1987, Clair and Holbrook, 2017). For these research works, diffractions and reflections can be separated and the diffracted hyperbolae are migrated with suitable velocity band. The entropy or varimax values can reach to the extremes if environment velocity is chosen. Besides, energy difference technique developed by C. Le (Nguyen et al., 2017)

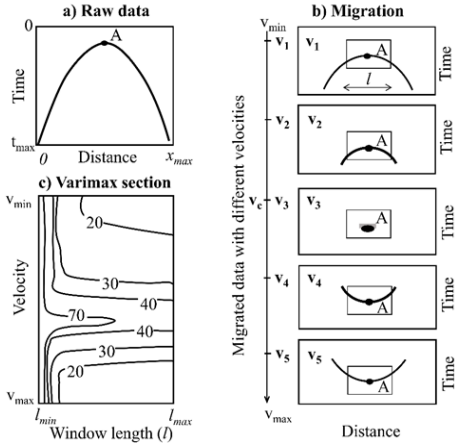

Fig. 1. Workflow for establishing a varimax section. a) Raw data, b) Migration. The raw data is migrated with different velocities. The migrated data can fall into one of three categories: under-migration, correct migration, and over-migration. If correct migration is, no "smiling" or "frown eyes" are recognized (Yilmaz, 2001). c) The varimax section is formed by representation of varimax depending two variables, window length and velocity. vc is the environment velocity.

Rys. 1. Przebieg pracy przy tworzeniu sekcji varimax. a) Surowe dane, b) Migracja. Surowe dane są migrowane z różnymi prędkościami. Migrowane dane mogą należeć do jednej z trzech kategorii: niepełna migracja, poprawna migracja i nadmierna migracja. Jeśli jest to poprawna migracja, nie rozpoznaje się „uśmiechu" lub „zmarszczenia brwi" (Yilmaz, 2001). c) Sekcja varimax jest utworzona przez przedstawienie varimax w zależności od dwóch zmiennych, długości i prędkości okna. vc jest prędkością środowiska.

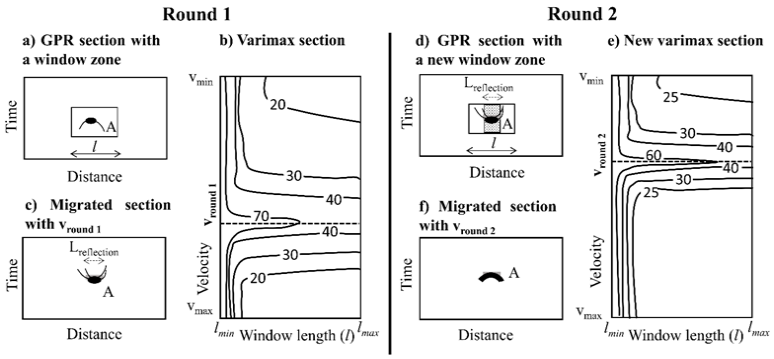

Fig. 2. Images of varimax sections (b and e) from two different window zones (a and d). For round 1, Figure c shows the over-migration effect coming from the higher migrated velocity than the environment velocity. For round 2, Figure f shows the focused image without over-migration effect after applying a new window zone without contribution of reflection (the dot area as $L_{reflection}$)

Rys. 2. Obrazy przekrojów varimax (b i e) z dwóch różnych stref okiennych (a i d). W rundzie 1 rysunek c pokazuje efekt nadmiernej migracji pochodzący z wyższej prędkości migracji niż prędkości otoczenia. W rundzie 2 rysunek f pokazuje zogniskowany obraz bez efektu nadmiernej migracji po zastosowaniu nowej strefy okna bez udziału odbicia (obszar kropki jako $L_{reflection}$)

can show that maximum energy difference can occur in the peak of diffraction hyperbolae with environment velocity applying to the GPR data

In this research, we develop a novel approach by combining the Kirchhoff migration and the diagram of GPR attributes to evaluate the environment velocity and underground anomalies' properties (i.e., their locations and their sizes). We will apply the approach in the GPR synthetic data and real data in Ba Ria-Vung Tau province, Vietnam.

2. Method

Analyzing expressions of GPR amplitudes in migrated sections with a velocity band can provide tools of velocity estimation. According to research works (Yilmaz, 2001, Nguyen et al., 2017) when GPR data is migrated with correct velocity, the diffraction hyperbola turns into highly energy point at its peak. If the migrated velocity is not correct, over-migration or under-migration effects can occur with higher velocity or lower velocity than the environment velocity, respectively (Figure 1). In the wrong velocity case, the GPR migrated amplitudes are still stretched in curved shapes upward or downward, causing highly entropy data (De Vries and Berkhout, 1984, Wiggins, 1978, Prego et al., 2017, Fomel et al., 2007, Levy and Oldenburg, 1987, Clair and Holbrook, 2017). For these research works, the varimax and its inverse, entropy, within window zone containing the peak of diffraction hyperbola can also reach maximum or minimum, respectively.

Three functions of GPR migrated amplitude, varimax, entropy, and energy, are our interest. Varimax and entropy can relate to chaos degree of the GPR amplitude. For the energy variable, we are interested in investigating its strength over the reflection or diffraction events. Relationship between the GPR attributes (i.e., varimax, entropy, and energy) over two variables as velocity and a window can be of great explanation of the environment velocity. Also, we can investigate how useful the energy attribute can contribute to the velocity estimation from the small diffractor.

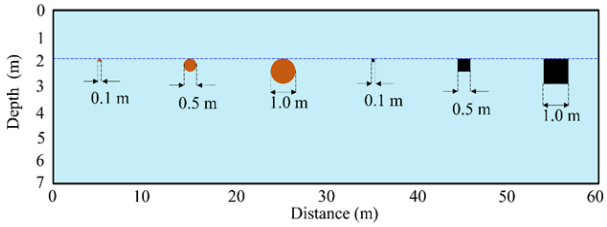

Fig. 3. Model of six anomalies in Cartesian coordinates including three solid circles and three solid squares
Rys. 3. Model sześciu anomalii we współrzędnych kartezjańskich, w tym trzy ciągłe koła i trzy ciągłe kwadraty

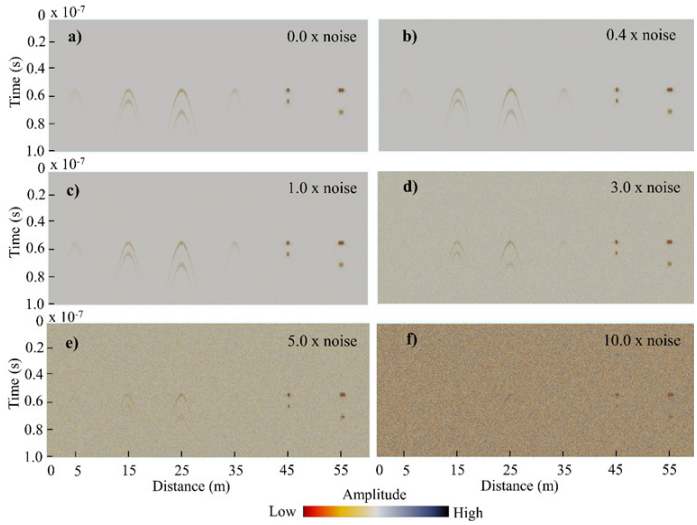

Fig. 4. The synthetic dataset with different Gaussian noise levels expressed as the parameter, constant_value. a) no Gaussian noise added, b) 0.4 Gaussian noise added, c) 1 Gaussian noise added, d) 3 Gaussian noise added, e) 5 Gaussian noise added, f) 10 Gaussian noise added
Rys. 4. Syntetyczny zestaw danych z różnymi poziomami szumu Gaussa wyrażonymi jako parametr, stała wartość. a) bez dodanego hałasu Gaussa, b) 0,4 dodanego hałasu Gaussa, c) 1 dodanego hałasu Gaussa, d) 3 dodanego hałasu Gaussa, e) 5 dodanego hałasu Gaussa, f) 10 dodanego hałasu Gaussa

2.1. Analysis of GPR attributes

Building GPR attribute diagram needs a set of migrated GPR sections from a velocity band in advanced. The extremes of the GPR attribute (i.e., entropy, energy, and varimax) can reflect to the suitable environment velocity (Fomel et al., 2007, Clair and Holbrook, 2017). Each GPR attribute is formed using two variables, velocity and window zone through its equation as followed:

(i) For the chaos of the GPR migrated data, entropy definition is introduced (Sava et al., 2004):

(ii)

$$Entropy = \frac{(\Sigma_i \Sigma s_i^2)^2}{\Sigma_i s_i^4} \quad (1)$$

(iii) For the inverse of the entropy, varimax term is used for minimum the order of "spikiness" or detecting the smallest number of the largest spikes as the equation (Wiggins, 1978):

(iv)

$$Varimax = \frac{\Sigma_i s_i^4}{(\Sigma_i \Sigma s_i^2)^2} \quad (2)$$

(v) We tempted to add one more energy term for researching the chaos level of migrated data as the equation (dGB Earth Sciences, 2015):

(vi)

$$Energy = \Sigma_i s_i^2 \quad (3)$$

where, s_i is an amplitude in a GPR migrated section with a defined velocity. i is the location of the data point within the window zone. The flowchart for one example of a GPR attribute versus two variables, velocity, and window length (i.e., varimax) is expressed in the Figure 1.

The rectangular window zone has width as time distance in nanosecond and length as distance in meter covering the peak of the diffracted hyperbola. The maximum varimax can show the chosen velocity in which its migrated data show the smalless number of spikiness (Wiggins, 1978).

2.2. The new technique: varimax diagrams made by from the diffraction contribution

We have developed a new workflow of calculating varimax section for defining environment velocity and size of an object. For small objects, the conventional workflow (Fomel et al., 2007, Clair and Holbrook, 2017) expresses that maximum varimax value in a full rectangular window can relate to environment velocity. Apparently, maximum varimax values can lead to smallest number of spikiness in the window area of the GPR migrated data. That is, the diffracted hyperbola can converge into the focus point. However, the focus data point cannot answer to the full size of the big object. For the big object, our technique can calculate contribution of diffracted GPR waves in varimax diagram in which the maximum varimax responds to the environment velocity.

We apply the idea of achieving smallest number of spikiness of the GPR data after mitigating diffraction effects. For

the big object, there can be two separated zones, (i) zone being responsible for reflection effect and (ii) zone for diffraction effect. Then, after removal of reflection zone, the diffraction zone can converge into the stage of being the smallest number of spikiness of the GPR data with the suitable velocity responding to the max varimax parameter. Note that exact separation of reflection and diffraction is a big challenge (Fomel et al., 2007).

Our workflow described in Figure 2 shows that two different varimax sections with two different window zones can produce two different velocities. Our technique needs three main processing factors: (i) calculation of a varimax diagram within a designated window zone from different migrated sections, (ii) the migrated section with velocity corresponding to the maximum varimax can give the object size, and (iii) condition for stopping the workflow depends on how dynamic characteristics of migrated events appear.

If correct migration occurs, the workflow stops. In case, over-migration case occurs, the new designated window zone does not include the reflection size of the object and a new varimax diagram is re-calculated. The full window zone shown in Figure 2a leads to the over-migrated image (Figure 2c). The new window zone (Figure 2d) for recalculating the varimax section (Figure 2e) is achieved by subtraction the full window zone from the zone defined as $L_{reflection}$. $L_{reflection}$ is got from the object size in the over-migrated image (Figure 2c). With the new varimax section, the migrated section (Figure 2f) shows the more focused object image.

3. Results

3.1 Numerical model

3.1.1. Building synthetic data

Setup model: The model includes six anomalies, three rectangular pipes and three circle pipes (Figure 3). In the model, the background velocity is 0.075 m/ns (equally, 0.75 x108 m/s) and its anomalies' ones is 0.122 m/ns (equally, 1.22 x108 m/s). The top of all the anomalies are in the same depth, 2 meter. Each anomaly type, circle or rectangular, has sizes as 0.1 m, 0.5 m, and 1 m.

Forward modelling: The modelling tool of the source code MATGPR (Tzanis, 2006, Tzanis, 2010) is used to build constant offset (CO) GPR data from the model (Figure 3). The tool utilized the modelling work of Bitri and Grandjean (1998) in which a phase shift technique in frequency-wavenumber domain and solution of 2D Maxwell 's equations is used for wavefield extrapolation.

We have added different noise levels into the synthetic GPR data for testing robustness and effectiveness of our workflow. The *newdata* combining modelled signal and noise contributions is formed by the equation:

*New_data=synthetic_data + constant_value * white_gausian_noise*

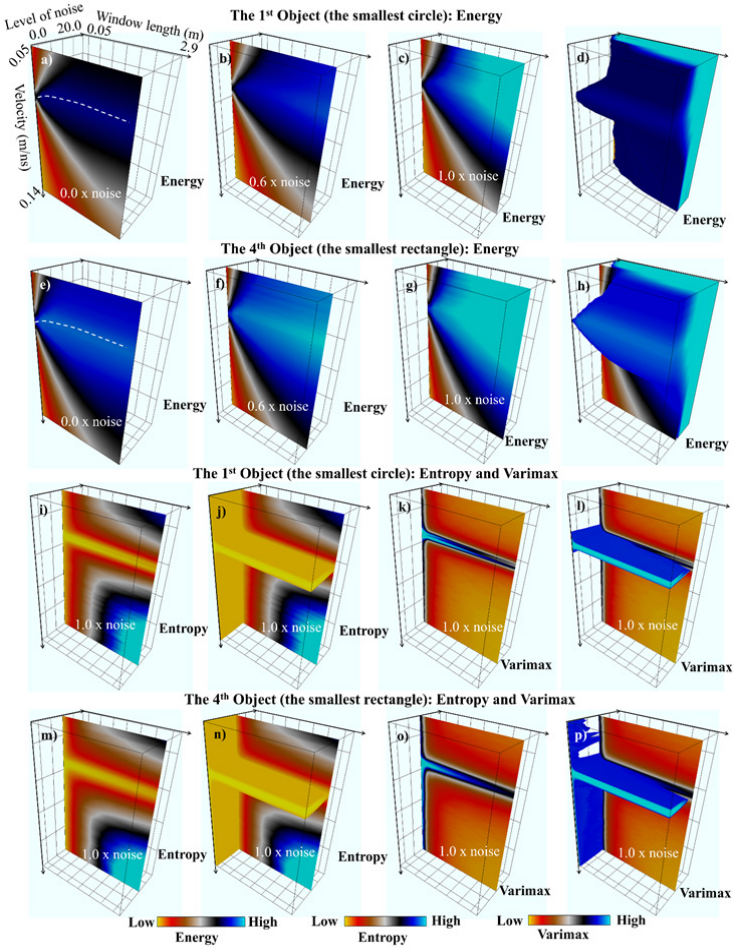

Fig. 5. Representations of energy, entropy, and varimax sections from synthetic datasets with different noise level for the smallest objects of cirlce and rectangle
Rys. 5. Reprezentacje sekcji energii, entropii i varimax z syntetycznych zestawów danych o różnym poziomie hałasu dla najmniejszych obiektów wiru i prostokąta

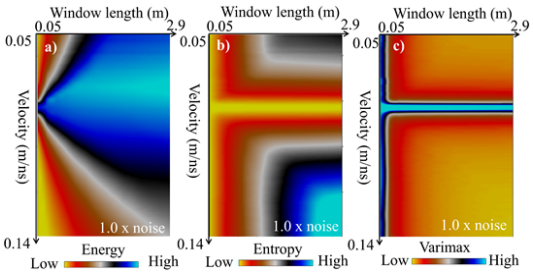

Fig. 6. Energy (a), entropy (b), and varimax (c) representations for the largest circle pipe (the third object) in the model
Rys. 6. Reprezentacje energii (a), entropii (b) i varimax (c) dla największej rury (trzeciego obiektu) w modelu

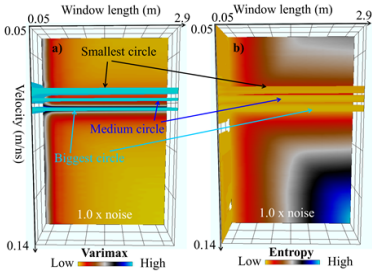

Fig. 7. 3D representations of varimax (a) and entropy (b) from synthetic dataset of 100% noise level added. The 2D varimax overlay accounts for the largest circle. The 3D bars of two circles (the medium and biggest) express the strong values of entropy and varimax are not equivalent to the environment velocity
Rys. 7. Reprezentacje 3D varimax (a) i entropii (b) z syntetycznego zestawu danych o dodanym poziomie hałasu 100%. Nakładka 2D varimax stanowi największy okrąg. Słupki 3D dwóch kół (średnie i największe) wyrażają wysokie wartości entropii, a varimax nie są równoważne prędkości otoczenia

Where, synthetic signal data is calculated from the source MATGPR; *constant_value* has values as 0.0, 0.2, 0.4, 0.6, 0.8, 1, 3, 5, 10, 20. The parameter, *white_gausian_noise*, is white Gaussian noise made by the Matlab built-in function (MathWorks, 2019), randn.m.

Figure 4 represents modelling data behavior from the model (Figure 3) with different noise addition levels defined as parameter *constant_value*. In a location of each circle (i.e., in the distances as 5, 15, 25 m), two separated hyperbolae express its top and bottom. Many other hyperbolae with the weaker amplitudes are formed by small diffractors locating at its left and right circular edges. Sizes of the strong-amplitude hyperbolae (in the distances 5, 15, and 25 m) increase depending on the sizes of the circular pipes. For the smallest rectangular pipe (in the distances 35 m), it shares the same hyperbolae shapes for top and bottom with the smallest circle pipe (in the distance 5 m). In the other bigger rectangular pipe (its center point at the distance 45 or 55 m), two horizontal layers with the four hyperbolae locating at each of the four corners are shown.

3.1.2. Processing and result

Our workflow using varimax section analysis is applied into three cases for the synthetic dataset (i) small objects including circle or rectangular pipes having diameter size as 0.1 m, (ii) big-sized circle (i.e., its diameter as 1 m), and (iii) big-sized rectangle (i.e., its diameter as 1 m). We would apply two routines for calculating environment velocity, (i) conventional and (ii) our suggest ones. For the other medium-sized objects as 0.5 m, we would compare their migrated results from the two routines with the discussed model in Figure 3.

Preparation for our varimax analysis, migrated sections with different velocities and survey settings in the OpendTect software (dGB Earth Sciences, 2015, Huck, 2012) are set up. All the GPR CO datasets are migrated with the velocity band ranging from 0.05 to 0.14 m/ns. For speeding migration process, parallel computing with four cores is applied in the calculation. The processor is Intel (R) Core™ i7-6700HQ CPU at 2.6 GHz in baseline running. Window length ranges from 0.05 m to 2.9 m horizontally and 6.35 ns vertically. The datasets consist of the pure synthetic data and different white Gaussian noise addition levels. Therefore, each 3D varimax is built up with three dimensions, velocity, window length, and level of noise (white Gaussian noise addition level) defined as *constant_value*. For 3D view, inline and crossline are nonlinearly defined as window length and level of noise, respectively. The velocity is linearly expressed as Z direction.

We applied analysis of attribute diagrams for three cases in the model (Figure 3); (i) the smallest objects with the first object for the smallest circular pipe and the fourth for smallest rectangular pipe, (ii) the largest circle object for the third, and (iii) The largest rectangular object for the sixth.

3.1.2.1 Conventional routine

Case 1: the small objects

The interest objects as small circles and rectangles with their diameters as 0.1 m, locate at the distances 5 m and 35 m, respectively. The three kinds of GPR attributes as energy, entropy and varimax are input for velocity estimation in an object. The window area for the attributes are full rectangles with the constant time gate (6.35 ns) and varied window length from 0.05 m to 2.9 m.

Figure 5 provides the diagrams of entropy, energy, and varimax for the small objects from the synthetic GPR data with different noise levels. In energy analysis, the maximum energy values responding to velocity changes versus the window length (i.e., see the dashed white curve) although good estimation for environment velocity just works well with the

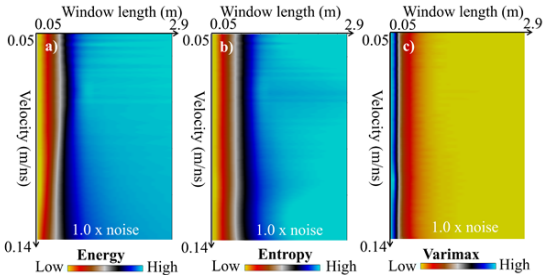

Fig. 8. Energy, entropy, and varimax sections from synthetic dataset of 100% noise level for the biggest rectangular object. All the sections cannot show the good estimate for environment velocity

Rys. 8. Sekcje energii, entropii i varimax z syntetycznego zestawu danych o poziomie hałasu 100% dla największego obiektu prostokątnego. Wszystkie sekcje nie dają dobrego oszacowania prędkości środowiska

smallest window length. Meanwhile, for entropy and varimax sections, the min entropy and max varimax are stably invariant reflecting the environment velocity even when window length and noise levels change. Their 3D representations also show their extremes (the furthest left image in Figure 5).

Case 2: the largest circle object

According to the representations of different GPR attributes for the largest circle object in Figure 6, the environment velocity is not correctly picked with the extreme values of the GPR attributes. It shows that the extreme values for the GPR energy section change due to the window length; meanwhile, the entropy or varimax cannot answer the environment velocity with their extreme values although they refer a constant velocity.

For analysis of entropy and varimax in the biggest circle object, the invariant velocity responding to the extreme values, minimum entropy or maximum varimax, is not equal to the environment velocity when the conventional workflow of full window zone covering the diffraction is applied. Figure 7 expresses three velocities corresponding to the extreme values shown by the three 3D entropy or varimax bars of the three circles objects. It illustrates that the chosen velocity relating to the extremes increases if the objects' sizes increase.

Case 3: The largest rectangular object

In Figure 8, all the three GPR attributes (energy, entropy, and varimax) do not show any visible extreme values responding to the environment velocity. It shows that the full rectangular window zone is not helpful for illuminating the differences of diffractions or reflection signal.

Figures 7 and 8 inspires us to try a new strategy in finding environment velocity from GPR diffracted signals of the biggest objects. For velocity estimation in traditionally window zone, some remarks are made; (i) energy sections cannot provide a good tool for velocity estimation, (ii) entropy or varimax for the circle type can show the constant velocity with different axis parameters but it is not the environment velocity if its object size is big, and (iii) entropy or varimax for the rectangular object type does not reflect any extreme values that connect to environment velocity.

3.1.2.2. Our new technique

Our new flowchart for defining environment velocity is provided (see Section 2.2). For analyzing velocity from the synthetic datasets, GPR data zone connecting to the biggest objects as circles and rectangles are discussed. Taking advantages of the migrated sections from the velocity band, several rounds of calculating 3D varimax distribution with contribution of diffraction are applied. The idea of the flowchart is that reflection contribution is removed out of the calculation of varimax and the extreme varimax will respond to the contribution of the diffraction.

Case 2: the largest circle object

We have worked with four rounds of calculating varimax sections (Figures 9 and 10) for achieving the environment velocity and its sizes. The first round comes up with the velocity 0.082 m/ns showing the maximum varimax and its migrated section shows over-migration effect. Many over-migration effect or upward curves in the migrated section (Figure 9c) shows that the chosen velocity bigger than the environment one. In the second round, its window zone does not include the reflection zone as 0.15 m which is extracted from the migrated section of the first round (Figure 9b). The second-round migrated section with the chosen velocity, 0.080 m/ns, also has over-migration effect (Figure 9d) although the object size increase to 0.36 m better than the previous result 0.15 m.

In the third round, the migrated section also has over-migration effect with the better results, the object size 0.51 m and the chosen velocity 0.078 m/ns. The best-chosen velocity is 0.076 m/ns and the object size as 0.95 m in the migrated section for the fourth round shows the acceptable errors, 1.3% and 5%, respectively. The migrated section (Figure 10f) show the focused result image.

Case 3: The largest rectangular object

Two rounds of calculating varimax sections is done for calculating the biggest rectangular size, 1 m and the environment velocity, 0.75 m/ns (Figure 11). The first round (Figure 11a) does not show any meaningful max varimax value that could help to define velocity or its migrated section. In the second round, reflection contribution of the rectangular pipe as 1.05 m is calculated from the synthetic GPR data (Figure 4) in advance. After removing the reflection contribution, the new varimax in the second round (Figure 11b) shows the great chosen velocity

3.2. Real data

The data was recorded in Ba Ria Vung Tau province, Vietnam for checking present map of two underground metal gas

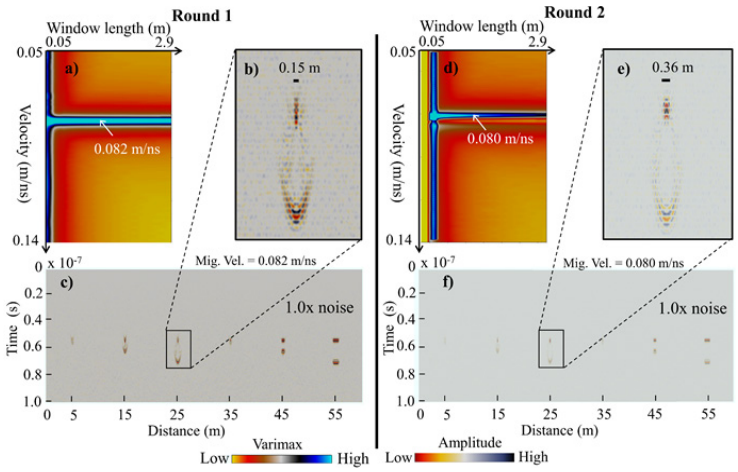

Fig. 9. Varimax and migrated sections with the chosen velocity for the max varimax from synthetic dataset of 1 noise level for the first and second rounds. The largest circle is accounted

Rys. 9. Varimax i sekcje z wybraną prędkością dla maksymalnego varimax z syntetycznego zestawu danych dla 1 poziomu hałasu dla pierwszej i drugiej rundy. Wyliczenia dla największego kręgu

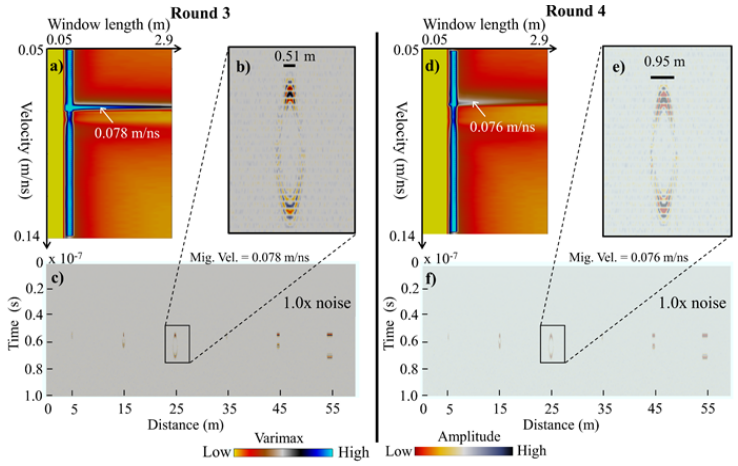

Fig. 10. Varimax and migrated sections with the chosen velocity for the max varimax from synthetic dataset of 1 noise level for the third and fourth rounds. The largest circle is accounted

Rys. 10. Varimax i sekcje z wybraną prędkością dla maksymalnego varimax z syntetycznego zestawu danych o poziomie hałasu 1 dla trzeciej i czwartej rundy. Wyliczenia dla największego kręgu

pipes. For prior information, two pipes have diameters as 0.66 m and 0.41 m for Nam Con Son (NCS) pipe and Bach Ho (BH) pipe, respectively (PV GAS, 2019). Two sign bars reflect their existence below the ground (Figure 12, left image). The GPR profile (Figure 12, right image) is collected across the two anomalous pipes using a Detector Duo IDS machine, Italy in 2019. Its configuration parameters include measurement length as 16.5 m, number of traces as 592 and the sample space on each trace as 0.25 ns. It follows the Constant Offset tradition. The data for analysis contains the central frequency as 700 MHz.

For preparation of the input data for our workflow, several processing techniques (Nguyen et al., 2017) are listed below: (i) Move start time: shifting the trace to the time zero, (ii) Removing the DC noise, (iii)Removing the background noise, (iv) Using dewow filter for low frequency removal, (v) Band-pass filter for frequencies from 350 MHz to 1050 MHz, and (vi) Gain filter to enhance weak signal in the big time.

Some brief interpretation can be extracted from the processed data (Figure 12, right image). A significant layer locates at the time 20 ns. Two strong symmetrical and unsymmetrical hyperbolae events related to diffraction effects at the two locations (x = 2 m, t = 30 ns) and (x = 9 m, t = 35 ns) can respond to the two underground metal gas pipes, NCS and BH, respectively. Our workflow of velocity estimation by the varimax diagrams (see Section 2.2) is applied to the first location where the symmetrical hyperbola peak is captured in distance-time domain, 2 meter and 30ns.

We have used our workflow to the real GPR data with different rounds (Figures 13 and 14).

- The first round:

In the first round (Figure 13), the varimax is established with velocity band from 0.08 m/ns to 0.16 m/ns and the window length from 0.05 to 2.9 m. Obviously, the largest window zone can cover the biggest pipe. The varimax section (Figure 13a) firstly shows the velocity corresponding to the max varimax (see white arrow) with different full window lengths. The zoom image extracted from the whole migrated section (Figure 13c) can illustrate several "smile curves" as over-migra-

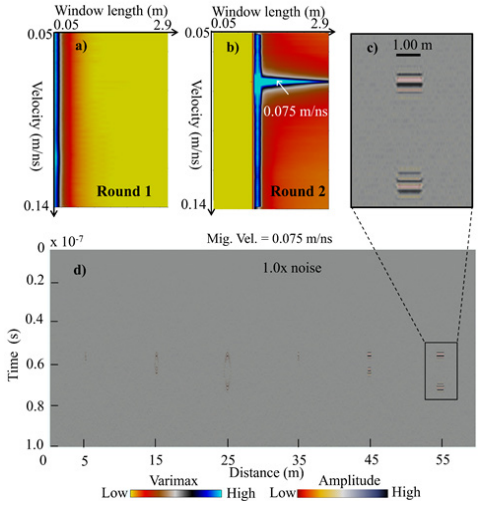

Fig. 11. Varimax (a and b) and migrated sections (c and d) with the chosen velocity of the max varimax from synthetic dataset of 100% noise level in the biggest rectangular object. The varimax section (a) in round 1 cannot show the estimate for velocity when it has contribution of the reflection and diffraction signals. The varimax section (b) from the new varimax technique after removal of reflection contribution can show the great estimate for the environment velocity

Rys. 11. Varimax (a i b) i migrowane sekcje (c i d) z wybraną prędkością maks. Varimax z syntetycznego zestawu danych o poziomie hałasu 100% w największym obiekcie prostokątnym. Sekcja varimax (a) w rundzie 1 nie pozwala na oszacowania prędkości z uwagi na udział odbicia i sygnały dyfrakcyjne. Sekcja varimax (b) z nowej techniki varimax po usunięciu udziału odbicia może wykazać świetne oszacowanie

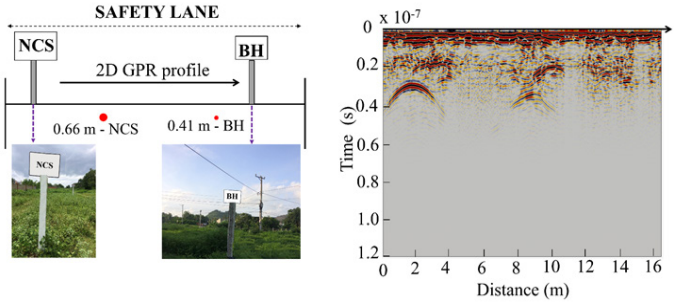

Fig. 12. Real site in Ba Ria – Vung Tau province, Vietnam (left image). The GPR measurement (right image) is to research anomalous objects and especially, existence of two gas metal pipes

Rys. 12. Realna lokalizacja Ba Ria - prowincja Vung Tau, Wietnam (lewy obraz). Pomiar GPR (prawy obraz) ma na celu zbadanie anomalnych obiektów, a zwłaszcza istnienia dwóch metalowych rur gazowych

tion effect. The migrated section (Figure 13c) with the chosen velocity, 0.115 m/ns can illustrate the size of the NCS metal pipe around 0.4 m.

- The second round:

The next step is to reevaluate the new varimax section with different window zones without the zone of reflection contribution that are defined the Figure 13b. In the Figure 13d, the varimax shows the velocity of the max varimax as 0.104 m/ns. Interestingly, the new migrated section (Figure 13e and f) expresses the new image result with having little over-migration effect and being more focused. We can compare its size, 0.61 m with the prior information, 0.66 m. The error percentage, 8%, is acceptable to confirm the validity of the method.

For further evaluation of velocity, we have tried the third round of calculating a new varimax section after extracting the reflection zone, 0.61 m from the second round (Figure 13e). The varimax section of the third round shows the velocity value as 0.096 m/ns (Figure 14a) and the object size as 0.8m (Figure 14b). The object image (Figure 14b) can remind us about the under-migration effect from the research works (Nguyen et al., 2017, Yilmaz, 2001, Holbrook et al., 2016).

4. Discussion

The synthetic datasets with different added error levels and real data are tested using varimax diagrams. The testing shows that using varimax sections can define the environment velocity.

For small objects, the traditional entropy or varimax diagram shows their great applications in velocity estimation. The reason is that diffraction mainly comes from the small objects.

In big circle object's cases, traditional rectangular window for a zone of hyperbola can lead to the over-migrated effect with its resulted velocity. It could be explained when Kirchhoff migration sum all the amplitude locating in the hyperbola curve of diffraction, it assumes the circular shape of the object as a part of its diffracted hyperbola and turns circle the shape into the focused point.

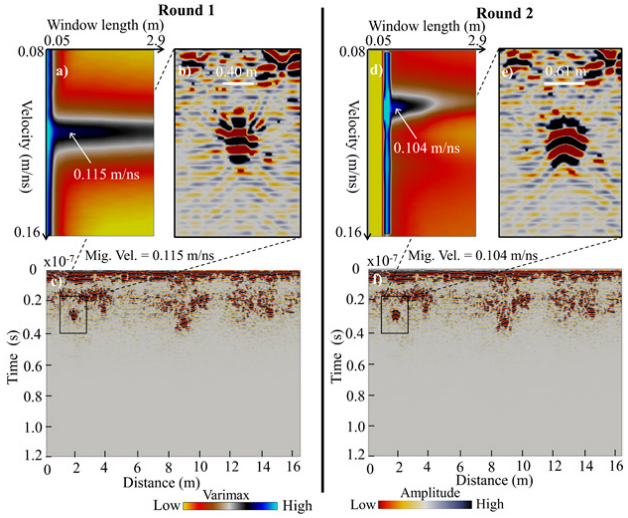

Fig. 13. Varimax (a and d) and migrated sections (c and f) with the chosen velocity of the max varimax in the real data (rounds 1 and 2). The varimax (a) in round 1 cannot show the environment velocity from over-migration effects in the migrated section (b). The varimax (d) in round 2 can show the environment velocity from the migrated section (f) of highly focused image

Rys. 13. Varimax (a id) i migrowane odcinki (c i f) z wybraną prędkością maks. Varimax w danych rzeczywistych (rundy 1 i 2). Varimax (a) w rundzie 1 nie może wykazuje zależności prędkości środowiska od efektów migracji w sekcji (b). Varimax (d) w rundzie 2 może wykazuje prędkość środowiska z migrowanej sekcji (f) silnie zogniskowanego obrazu

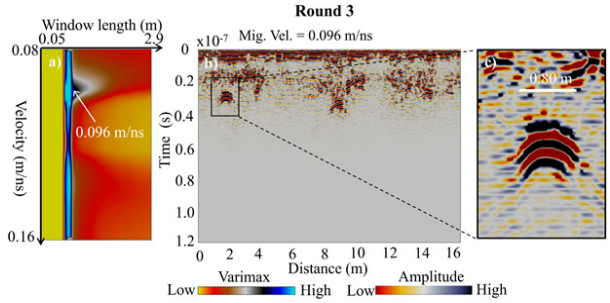

Fig. 14. Varimax and migrated sections with the chosen velocity for the real data for round 3. The varimax section (a) in round 3 cannot show the environment velocity because of under-migration effects in the migrated section (b and c)

Rys. 14. Varimax i migrowane sekcje z wybraną prędkością dla danych rzeczywistych dla rundy 3. Sekcja varimax (a) w rundzie 3 nie wykazuje prędkości środowiska z powodu efektów poniżej migracji w migrowanej sekcji (b i c)

For the big rectangular pipe, the tradition full rectangular window cannot be well applied. The energy, entropy and varimax do show no extreme values that could relate to the velocity.

In our suggested workflow, the varimax diagram without reflection contribution can reveal the strongest varimax responding to the environment velocity. The reflection contribution can be defined from migrated GPR sections.

5. Conclusion

We have applied the traditional workflow and our workflow of velocity estimation by using varimax diagrams to the synthetic and real data. For small objects, the both workflows could provide the environment velocity. However, in the big object case our workflow can work better than the tradition one when our new varimax sections with a suitable window setting can catch diffraction contribution after removal of reflection contribution. Moreover, the categories of over-migration, correct migration, and under-migration is the stop condition of our workflow. Finally, energy diagram does not show its effectiveness in detecting environment velocity because the instability of energy extremes occurs with different window lengths.

6. Acknowledgments

This research is funded by Vietnam National University HoChiMinh City (VNU-HCM) under grant number C2019-18-08. I would like to thank Anh L. T. Ha for her support.

Literatura – References

1. BITRI, A. & GRANDJEAN, G. 1998. Frequency–wavenumber modelling and migration of 2D GPR data in moderately heterogeneous dispersive media. Geophysical Prospecting, 46, 287-301.
2. CHOPRA, S. & MARFURT, K. J. 2007. Seismic attributes for prospect identification and reservoir characteriztion, United States of America, Tulsa, Okla. (8801 South Yale St., Tulsa OK 74137-3175) : Society of Exploration Geophysicists
3. CLAIR, J. S. & HOLBROOK, W. S. 2017. Measuring snow water equivalent from common-offset GPR records through migration velocity analysis. The Cryosphere, 11, 2997-3009.
4. DE VRIES, D. & BERKHOUT, A. 1984. Velocity analysis based on minimum entropy. Geophysics, 49, 2132-2142.
5. DGB EARTH SCIENCES. 2015. OpendTect dGB Plugins User Documentation version 4.6 [Online]. Available: http://opendtect.org/relman/4.6.0/unpacked/4.6.0/doc/User/dgb/chapter2.3_attributes_with_steering.htm.
6. DOOLITTLE, J. A. & COLLINS, M. E. 1995. Use of soil information to determine application of ground penetrating radar. Journal of Applied Geophysics, 33, 101-108.
7. ERCOLI, M., PAUSELLI, C., FRIGERI, A., FORTE, E. & FEDERICO, C. 2014. 3-D GPR data analysis for high-resolution imaging of shallow subsurface faults: the Mt Vettore case study (Central Apennines, Italy). Geophysical Journal International, 198, 609-621.
8. FOMEL, S., LANDA, E. & TANER, M. T. 2007. Poststack velocity analysis by separation and imaging of seismic diffractions. Geophysics, 72, U89-U94.
9. FORTE, E., DOSSI, M., PIPAN, M. & COLUCCI, R. 2014. Velocity analysis from common offset GPR data inversion: theory and application to synthetic and real data. Geophysical Journal International, ggu103.
10. HOLBROOK, W. S., MILLER, S. N. & PROVART, M. A. 2016. Estimating snow water equivalent over long mountain transects using snowmobile-mounted ground-penetrating radarSnow water equivalent from GPR. Geophysics, 81, WA183-WA193.
11. HUCK, H. 2012. The road to open source: Sharing a ten years' experience in building OpendTect, the open source seismic interpretation software. 74th EAGE Conference and Exhibition. Copenhagen, Denmark.
12. KHOSHNAVAZ, M. J., BÓNA, A. & UROSEVIC, M. 2016. Velocity-independent estimation of kinematic attributes in vertical transverse isotropy media using local slopes and predictive paintingVelocity-less estimation of attributes. Geophysics, 81, U73-U85.
13. LE, C. V. A., HARRIS, B. D. & PETHICK, A. M. 2019. New perspectives on Solid Earth Geology from Seismic Texture to Cooperative Inversion. Scientific Reports, 9, 14737.
14. LEVY, S. & OLDENBURG, D. 1987. Automatic phase correction of common-midpoint stacked data. Geophysics, 52, 51-59.
15. MATHWORKS. 2019. Normally distributed random numbers [Online]. Available: https://www.mathworks.com/help/matlab/ref/randn.html 2020].
16. NGUYEN, T. V., LE, C. V. A., NGUYEN, V. T., DANG, T. H., VO, T. M. & VO, L. N. L. Energy Analysis in Semiautomatic and Automatic Velocity Estimation for Ground Penetrating Radar Data in Urban Areas: Case Study in Ho Chi Minh City, Vietnam. International Conference on Geo-Spatial Technologies and Earth resources, 2017 Ha Noi, Vietnam. Springer.
17. PREGO, F., SOLLA, M., PUENTE, I. & ARIAS, P. 2017. Efficient GPR data acquisition to detect underground pipes. NDT & E International, 91, 22-31.
18. PV GAS. 2019. PV GAS signed contracts belonging to the revised "Nam Con Son 2 Gas Pipeline" Project, "Sao Vang – Dai Nguyet Gas Pipeline" Project [Online]. Available: https://www.pvgas.com.vn/en-us/news/pv-gas-signed-contracts-belonging-to-the-revised-nam-con-son-2-gas-pipeline-project-sao-vang-dai-nguyet-gas-pipeline-project [Accessed January 6th, 2020.
19. SAVA, P., BIONDI, B. & ETGEN, J. 2004. Diffraction-focusing migration velocity analysis with application to seismic and GPR data. Stanford Exploration Project report-115.
20. SHAM, J. F. & LAI, W. W. 2016. Development of a new algorithm for accurate estimation of GPR's wave propagation velocity by common-offset survey method. NDT & E International, 83, 104-113.
21. SMITH, D. G. & JOL, H. M. 1995. Ground penetrating radar: antenna frequencies and maximum probable depths of penetration in Quaternary sediments. Journal of Applied Geophysics, 33, 93-100.
22. TOMECKA-SUCHOŃ, S. & MARCAK, H. 2015. Interpretation of ground penetrating radar attributes in identifying the risk of mining subsidence. Archives of Mining Sciences, 60, 645-656.

23. TZANIS, A. MATGPR: A freeware MATLAB package for the analysis of common-offset GPR data. Geophysical Research Abstracts, 2006.

24. TZANIS, A. 2010. matGPR Release 2: A freeware MATLAB® package for the analysis & interpretation of common and single offset GPR data. FastTimes, 15, 17-43.

25. WIGGINS, R. A. 1978. Minimum entropy deconvolution. Geoexploration, 16, 21-35.

26. YILMAZ, O. 2001. Seismic Data Analysis: Processing, Inversion, and Interpretation of Seismic Data, United States of America, Society of Exploration Geophysicists.

27. ZHAO, W., TIAN, G., FORTE, E., PIPAN, M., WANG, Y., LI, X., SHI, Z. & LIU, H. 2015. Advances in GPR data acquisition and analysis for archaeology. Geophysical Journal International, 202, 62-71.

Wykrywanie anomalii podziemnych za pomocą analizy wskazań radaru penetrującego ziemię

Konieczność określenia parametrów podziemnych budowli ma na celu wytyczanie dalszych zadań, takich jak konserwacja, naprawa lub ustawianie nowych konstrukcji podziemnych. Dla tych potrzeb radar penetrujący ziemię, jedna z wydajnych metod geofizycznych, pozwala osiągnąć wysoką rozdzielczość podziemnego obrazu ukazującego istnienie zarówno naturalnych jak i sztucznych anomalii. Stałe ustawienie anten odbiornika i nadajnika jest powszechnie stosowane na obszarach miejskich. Konwencjonalnie opis za pomocą hiperboli jest kluczowym wskaźnikiem rozproszenia obiektów, takich jak rury, system odprowadzania wody i betonowe konstrukcje budowlane, a także ujścia wody. Obliczanie ich głębokości i rozmiarów wymaga analizy migracji w środowisku. Migracja o różnej prędkości pokazuje różne stopnie transformacji od krzywej dyfrakcji do jej zogniskowanego obszaru. Przebadano diagramy różnych nastawień radaru penetrującego grunt, takich jak energia, entropia i varimax, zależnych od dwóch zmiennych, prędkości i parametrów okna obejmującego dyfrakcję dla zestawu danych syntetycznych i danych rzeczywistych. Opracowano nową technikę oceny prędkości w gruncie i wielkości obiektu poprzez połączenie nowego diagramu varimax i metody migracji Kirchhoffa. Technika taka może zdefiniować udział fal radarowych w ugiętym gruncie na podstawie diagramu po usunięciu udziału odbicia. Syntetyczne zestawy danych składają się z różnych losowych poziomów hałasu tła i różnej wielkości rur okrągłych i prostokątnych. Rzeczywiste dane są mierzone w celu wykrycia dwóch podziemnych rur gazowych w Ba Ria – prowincja Vung Tau, Wietnam

Słowa kluczowe: *migracja, szacowanie prędkości, wskaźniki radaru penetrującego ziemię*